Environmental Science
Water Research & Technology

PAPER

Cite this: *Environ. Sci.: Water Res. Technol.*, 2019, **5**, 944

Rejection of micron-sized particles using beech wood xylem†

Selin Vitas,[ab] Paul Beckmann,[c] Bertram Skibinski,[cd] Christian Goldhahn,[ab] Livius F. Muff[ab] and Etienne Cabane[*ab]

Received 30th October 2018,
Accepted 19th March 2019

DOI: 10.1039/c8ew00774h

rsc.li/es-water

The rejection of micron-sized particles mimicking the size of microorganisms responsible for waterborne diseases (such as *protozoans*) by filters made of wood tissue has been investigated in a dead-end filtration setup. The permeability reached up to 12 000 L m^{-2} h^{-1} per bar but a great variability has been observed for the wood filters. The swelling of the samples has been found to be the reason for the drop in permeability over long-term experiments (8 h). After drying the filter for 24 h at 65 °C, the initial permeability could be recovered, hence, this behaviour is reversible. The surrogates used in this study have a size of 5 and 20 μm and their electrostatic properties exclude potential electrostatic interactions. Hence, the removal of the particles occurs only through physical sieving. Microscopy investigations suggest that the surface of the wood as well as anatomical features, such as perforations, contribute to the removal of the particles. The log-removal value (LRV) of the filter depended on the size of the surrogates. In addition, the formation of a filter cake increased the LRV over time for both particle sizes used in this study. A prediction of the LRV has been calculated based on the pore size distribution of the filter rendered by image analysis. The results of the prediction are in accordance with the experimental observations.

Water impact

We propose to use wood, a bio-sourced material, as an alternative to synthetic polymers used for microfiltration membranes. Beech has interesting structural properties that might be used for filtration. We show that surface roughness and porosity contribute to the removal of suspended particles. Our results open up new in-sights for low-tech water facilities, possibly increasing the access to improved water.

1. Introduction

Water purification often uses filtration processes to remove particles, microorganisms, viruses or macromolecules from water. When compared to other conventional separation processes, such as sand filtration, membrane filtration offers a lot of advantages including compact modular design, low energy consumption, high productivity, moderate cost to performance ratio, and high selectivity.[1–3] Membranes are fabricated from a wide variety of organic (*e.g.* carbons, polymers) or inorganic (*e.g.* zeolites *etc.*) materials, with the vast majority of commercial membranes being made from polymers.[2,4,5] However, the production processes of polymer membranes often require chemical treatments using solvents, additives and etching agents.[6–8] The waste produced when preparing these membranes generates new environmental challenges. Therefore, it is important to develop membrane and filter materials with high separation efficiencies that are made from bio-sourced materials and manufactured with environmentally friendly processes. In this regard, natural materials such as wood and wood-based materials are considered as most promising candidates due to their renewability.[9–13]

Various agricultural and forestry waste, including wood, were used as biosorbents for the removal of heavy metals and organic contaminants.[14–19] Besides its adsorption capability, other studies report on the utilization of bulk wood for separation purposes in water purification, focusing on catalytic degradation of methylene blue and separation of oil and water.[9,20]

As of today, little is known about the removal efficiency of wood scaffolds for particulate material, especially in the size

[a] *Wood Materials Science, ETH Zürich, Stefano-Franscini-Platz 3, CH-8093 Zürich, Switzerland. E-mail: cabanee@ethz.ch*
[b] *Applied Wood Materials, EMPA – Swiss Federal Laboratories for Materials Science and Technology, Überlandstrasse 129, CH-8600 Dübendorf, Switzerland*
[c] *Chair of Water Supply Engineering, Technische Universität Dresden, 01062 Dresden, Germany*
[d] *Chair of Urban Water Systems Engineering, Technical University of Munich, Am Coulombwall 3, Garching 85748, Germany*

† Electronic supplementary information (ESI) available: A supplementary information file containing the ζ-potential of the surrogates, the scheme of the setup used for rejection experiments and the detailed description of the image analysis along with the original SEM images mentioned in the publication, as well as the spiking test for 5 μm particle is available. See DOI: 10.1039/c8ew00774h

range of water borne pathogens that are relevant in drinking water treatment, such as bacteria (0.5–3.8 μm, *e.g. E. coli*, *Pseudomonas aeruginosa*) and protozoa (4.9–12.2 μm, *e.g. Giardia* cysts, *Cryptosporidium* oocysts).[21,22]

The structure of hardwood consists of an anisotropic arrangement of cells, resulting in a material with directional porosity. This characteristic makes wood tissue particularly interesting for filtration in a continuous flow setup.[23] Wood consists of vessel channels and fibre channels, which are aligned along the growth direction.[24] Vessels are wide cells in hardwoods, which are specialised in the transport of water.[25,26] The vessel elements are usually about tens of micrometres in diameter, whereas the fibre elements have a diameter ranging from a few micrometres up to about 10 μm.[25] Individual cell elements do not exceed ~500 μm in length,[27] but they are connected end-to-end by perforation plates (which are either fully open or with micrometer sized pores), forming long vessel structures, which can reach meters in length.[25,28] This enables transport of water along the wood channels. Both vessels and fibres are interconnected with each other by pits on the channel walls. Water transport through those pits relies on capillary forces, which often limits the overall water transportation rate.[26] The porosity generated by the open lumina of vessels and fibres is therefore well adapted for the filtration of micron-sized objects, while the porosity of the cell wall (<100 nm) does not play a role in this size range.

As far as we know, these interesting features have been seldom investigated for water purification purposes. Freshly cut pine wood has been implemented in a dead-end filtration and was shown to remove dye and bacteria from water samples (Nile red and *Escherichia coli* were used as model pollutants).[29] Sens *et al.* investigated the application of two tropical hardwoods (caixeta and garapuvu) and one softwood (pine) for the treatment of water.[30] Two setups, dead-end filtration and helical cross-flow, were examined by filtering raw surface water. In the dead-end filtration mode, the system was hindered by significant pressure loss generated by the wood. In both studies, the authors used rather thick wood sections (in the longitudinal direction), which could have a significant influence on the flux.

Besides the macroscale geometry, the membrane pore size distribution has a critical influence on its applications as a filter medium.[31] The pore lengths, sizes, and distribution can vary a lot in between different wood species.[32] Besides the size of the openings present on the surface of a filtration material, its permeability is relevant. While the flow of water in softwood is supported by narrow cells only, the vessel network in hardwood is an evolutionary anatomical feature which promotes high flow rates within the tree. Based on this property, a common hardwood (beech, *Fagus sylvatica*) has been preferred over a softwood. Beech belongs to the semi-ring porous species, sometimes called diffuse porous, as the vessel elements are present throughout early and latewood but gradually decrease towards the year ring.[33,34]

The aim of this study is to evaluate the effectiveness of hardwood scaffolds for the removal of micron-sized particles (similar to protozoans diameters) under continuous flow. First, we characterised the beech wood cross-sections, through the determination of porosity parameters and ζ-potential measurements. The obtained quantities were used to predict the theoretical removal efficiency, based on structural considerations only. We then constructed a specific sample holder for the wood cross-section and a simple lab-scale setup to study the filtration characteristics. We determined parameters such as flux, permeability, and specific permeability and we assessed their time-dependency. Finally, the wood filter were challenged with micro-particles (5 μm and 20 μm in diameter) as surrogates for common microorganisms present in contaminated water. We showed that the wood filters are capable of removing particulate matter from a water stream in a continuous filtration setup. Moreover, we compared the experimental results with the theoretical prediction and discussed future improvements.

2. Material & methods

2.1. Experimental

2.1.1. Wood preparation. Beech and spruce wood are used in this study. The samples are cut into thin discs of dimensions ø 18 mm × 1 mm (ø RT × *L*, giving a specific flow area of 1.13 cm^2) using a circular saw. The samples are stored under controlled humidity conditions (65% moisture) until used. To test the reutilisation of the material after a long-time implementation, the samples are dried in an oven during 24 h at 65 °C and equilibrated in liquid media before being tested again.

2.1.2. Preparation of surrogate solutions. A solution of 0.01 M sodium chloride (NaCl) in water was used for all rejection experiments. Sodium chloride (NaCl) was purchased from Sigma Aldrich and dissolved in Milli-Q water. The pH of the solution was 6.1 ± 0.5.

Fluorescent silica microspheres (micromod Partikeltechnologie GmbH) have been used as model particles for the filtration experiments. Two sets of particles, which had diameters of 5 ± 1.5 μm and 20 ± 11.5 μm, were used. Their ζ-potential (as indicated by the supplier, data shown in Fig. S1†), is constant around −25 mV for pH values from 6 to 10. They exhibit isoelectric points at pH values of 4.01 (5 μm) and 4.21 (20 μm).

These particles were chosen because their sizes are similar to macro-sized water pollutants like protozoans, and because they are electronegative, like most naturally occurring particles in polluted surface waters. The particles have been suspended in the matrix solution in order to yield the surrogate solutions, with final concentrations of 10^6 particles per mL (5 μm) and 5×10^5 particles per mL (20 μm).

2.1.3. Rejection experiments. A bench-scale setup operating in the dead-end mode has been built (Fig. S2a†). The feed consists in two tanks; one containing Mili-Q water and the other one the surrogate stock solution under continuous stirring. In order to provide a constant flow from the closed feed tank, the container has been designed following the principle of a

Marriott's bottle.[35,36] A sampling point has been implemented before the filter. A custom-made filter holder has been developed in order to mount the filter into the setup (see Fig. S2b†). Native beech wood has been implemented in the setup perpendicularly to the flow for testing.

Each experiment begins with flushing the whole system with Mili-Q water from the feed water tank during 10 min at a flux of 8.0 L h^{-1}, which is measured through a magnetic inductive flowmeter (HygienicMaster, ABB). The rejection experiments are conducted following a spiking method developed by Van Hoof *et al.*[37] After the 10 min flushing, the inlet is switched from the water tank to the surrogate container.

The filtration capacity of the filter has been assessed by flowing the particles suspension through the filter during 30 min at a constant flowrate of 8 L h^{-1}. Samples at the permeate side were collected throughout the experiment. During the first five minutes, samples were taken every minute, then, every two and a half minutes. The efficiency of the filter was assessed by calculating the log removal value (LRV) with the following eqn (1).[38]

$$\mathrm{LRV} = \log_{10}\left(\frac{c_\mathrm{f}}{c_\mathrm{p}}\right) \quad (1)$$

where c_f is the particle concentration of the feed (inlet) and c_p the particle concentration of the permeate (outlet).

2.2. Analysis

2.2.1. Pore size distribution

Image analysis. Cross-sections of beech wood for SEM measurements were prepared with a rotary microtome (RM2255, Leica) equipped with a steel knife. SEM-micrographs were acquired with a Quanta 200 F from FEI in low vacuum mode, with an acceleration voltage of 10 kV. The SEM images of three distinct samples have been recorded on three different regions: earlywood, latewood and a transition zone (year ring), see Fig. S3 to S5.†

To determine the pore size, these images were analysed with the image analysis software ImageJ (version 1.52a), based on other studies[39–41] (detailed procedure can be found in the ESI†). The image analysis gives a pore number distribution, which can be used to calculate the mean pore size of the filter, d_pore, according to eqn (2).[42]

$$d_\mathrm{pore} = \sqrt{\left[\frac{\sum_{i=1}^{n} n_i {d_\mathrm{pore},i}^{2}}{\sum_{i=1}^{n} n_i}\right]} \quad (2)$$

where n is the total pore number, n_i and $d_{pore,i}$ are the pore number and diameter of an i-sized pore.

Intrusion porosimetry. The porosity of beech cross-sections were analysed through mercury intrusion porosimetry (MIP). Pores ranging from 3.5 nm up to 100 μm can be measured although the limit of the measurement is determined by the geometry of the sample. The samples were cut in small pieces 2 mm × 2 mm and analysed with a Pascal 140 + 440 instrument from POROTEC. The measurement has been carried out according to experimental conditions described in previous work.[32,43] Further details on the determination of the pore volume can be found in the ESI.†

2.2.2. pH resolved ζ-potential. Beech disks of 13.5 mm diameter and 6 mm thickness were obtained by cutting wood in conditioned state (20 °C and 65% relative moisture for minimum 48 h). Potassium chloride, KCl, Suprapur® with 99.999 purity (Merck, Switzerland) was dissolved in ultrapure water (18.2 MΩ cm^{-1}) to obtain the 1 mM KCl electrolyte measuring solution. 1 M titration solutions of sodium hydroxide (NaOH) and hydrochloric acid (HCl), Titrapure®, were purchased from Merck, Switzerland.

Conditioned beech disk samples were mounted in the cylindrical cell as described by Muff *et al.*[44] Note that the wooden disk sample was prepared and mounted such that the electrolyte flow was forced mainly through the sample in longitudinal direction, allowing probing the lumen surfaces. Streaming potential was measured with a 1 mM KCl solution in a SurPASS electrokinetic analyzer equipped with an automated titration unit from Anton Paar, Austria. The average streaming potential of four pressure ramps up to 400 mbar (two in each flow direction) was used to calculate the corresponding ζ-potential, shown in Fig. 1. The ζ-potential was calculated by the Attract 2.1 operating software from Anton Paar according to the Helmholtz–Smoluchowski equation.[45] The 1 mM KCl electrolyte solution was automatically titrated with a 1 M NaOH or HCl solution respectively, after every 4 pressure ramps.

2.2.3. Particle concentration. The concentration of the silica particles is determined through fluorescence measurement using a multimode plate reader (Infinite M200, Tecan) and employing a polystyrol well plate with a clear and flat bottom (black 96, Greiner Bio-One).

The samples are sonicated for 30 s to break up aggregates, then vortexed for 30 s for homogenisation. Thereafter, 100 μL of the solution are pipetted into the wells, in duplicate. Before each analysis, the well plates were shaken radially for 20 s in the plate reader to disperse the particles inside each well.

For fluorescence analysis, the suspension was excited at a wavelength of 485 nm, while the emission wavelength is measured at 510 nm. In total, five readings were recorded per well.

The calibration curves of the particle concentration were recorded in a 3-log concentration range, a linear behaviour over the total concentration range for both microspheres has been observed, as shown in Fig. 2. For the 5 μm silica particles, a 2-log concentration range is displayed resulting from the application of the statistical requirements limit of detection (LOD) and limit of quantification (LOQ), as described in DIN-32645 (2008).[46]

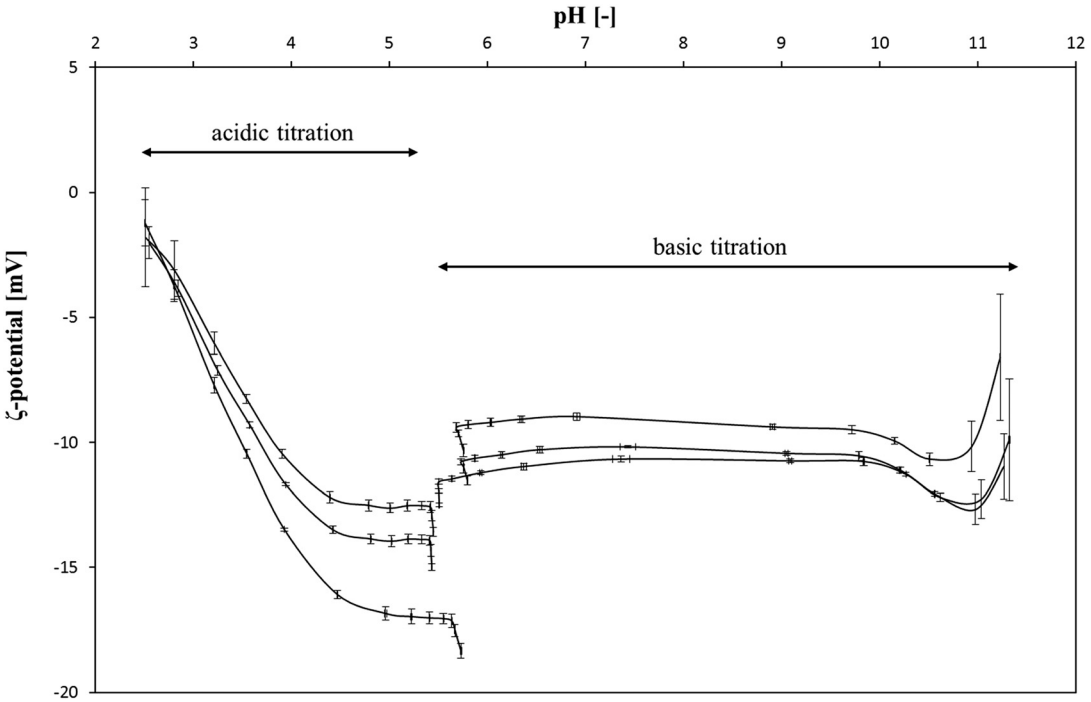

Fig. 1 ζ-Potential as a function of pH for six beech wood samples. Error bars represent the standard deviation of the measurement (n = 4).

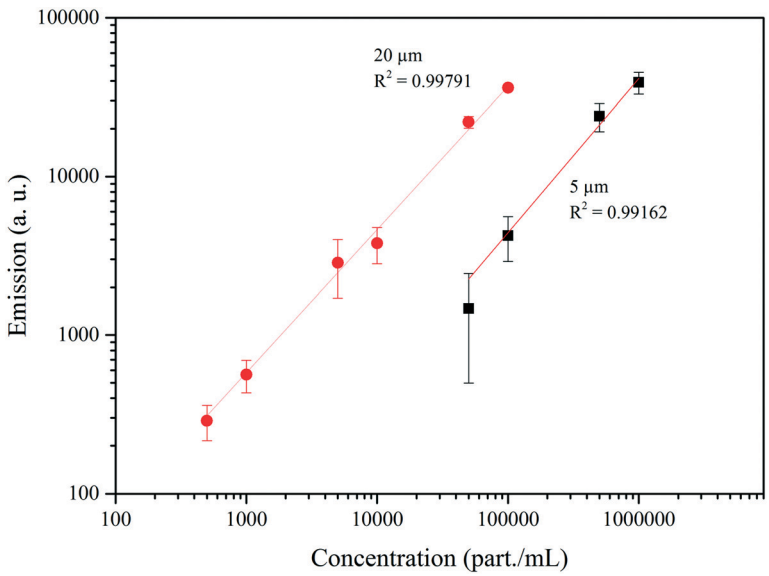

Fig. 2 Calibration curves of the fluorescent microspheres, error bars represent 95% confidence interval.

2.2.4. Predicted rejection by physical sieving. In order to predict the particle rejection through physical sieving alone, we have to exclude any other possible interactions. According to the ζ-potential measurements of the wood material (−10 mV) and the microspheres (−25 mV), a possible electrostatic interaction taking place during rejection experiment was not expected. By combining the pore size distribution of the filter with a quantitative expression for the passage of a particle, the fraction p of particles passing through the filter can be calculated following eqn (3):

$$p = \begin{cases} (1-\lambda)^2\left[2-(1-\lambda)^2\right]G; \lambda \le 1 \\ 0; \lambda > 1 \end{cases} \quad (3)$$

To use this equation, we assume cylindrical pores of diameter d_{pore}. Knowing the hydraulic particle diameter d_{hy}, the reduced particle radius λ can be calculated as follows:

$$\lambda = d_{hy}/d_{pore} \quad (4)$$

and G is the lag coefficient, estimated empirically by Zeman and Wales:[47]

$$G = \exp(-0.7146 \cdot \lambda^2) \quad (5)$$

The total particle passage p_t can be expressed as:

$$p_t = \sum_{i=1}^{n} p_i \frac{A_i}{A_{tot}} \quad (6)$$

Here, p_i describes the specific particle passage for the pore size i. The terms A_i/A_{tot} represents the relative contribution of the cross-sectional pore area of pore size i to the total cross-sectional pore area A_{tot}.

A simple relation between the total particle passage and a theoretical removal efficiency can be calculated:

$$LRV_{th} = \log_{10}\left(\frac{1}{p_t}\right) \quad (7)$$

3. Results and discussion

3.1. Pore size distribution of the wood filter

The analytical method described in chapter 2.2.1 has been applied on SEM images of the wood cross-section, such as the one shown in Fig. 3a. The black–white image yielded through the processing is shown on Fig. 3b. The pore number distribution and the mean cross-sectional pore area have been determined for the three regions (earlywood, latewood and transition zone) on each specimen, labelled S1, S2 and S3 on Fig. 3c.

The distribution of the cross-sectional pore-area (pore size) shows a bimodal curve. The first peak is centred on 10 μm and the second one is centred on 80 μm, corresponding to the characteristic pore size for both classes. These results correspond to the mean fibre and vessel size in beech wood, which have been found to be around 7 μm for the fibre and between 50–85 μm for the vessel.[48] The cumulative pore number distribution shows a steep increase until a pore size of 20 μm, thus, ~95% of the pores present on the samples are located within this pore size range, which correspond to the fibres and small vessels. The larger vessels account for 5% of the pores. For a semi-ring porous wood such as beech, the decreasing vessel diameters from earlywood to latewood is visible (see Fig. 3a). This explains the small variations in the cumulative pore number distribution for EW, LW and transition regions, visible between 25 and 75 μm.

As shown in the Fig. 3a and b, cluster of pores can be seen on the surface of the sample, formed by neighbouring vessel cells. Due to the thin cell wall in between them, they are often counted as one area during the image analysis, leading to an overestimation of large pores (>100 μm). As shown by Hass *et al.*, clusters in beech wood are more prominent in EW samples than in LW, which has also been observed in other studies.[49] Thus, the overestimation of large pores is more important in EW samples.

The mean pore size d_{pore} has been derived from the pore number distribution following eqn (2) and has been found to be 12.1 ± 1.3 μm, (errors represent the 95% confidence interval). This value account for all openings visible on the filter, some of them being vessels, which account for 31% of all cells in beech, and other are fibres, making up 37.4% percent of the cells.[25]

This value is comparable to coarse grain slow fixed-bed filters. They are usually packed with diatomaceous earth (DE), which has a median pore size of 13 μm.[50] This material is made of fossilised diatoms: microscopic unicellular aquatic plants widely present in the oceans.[51] It is mainly composed

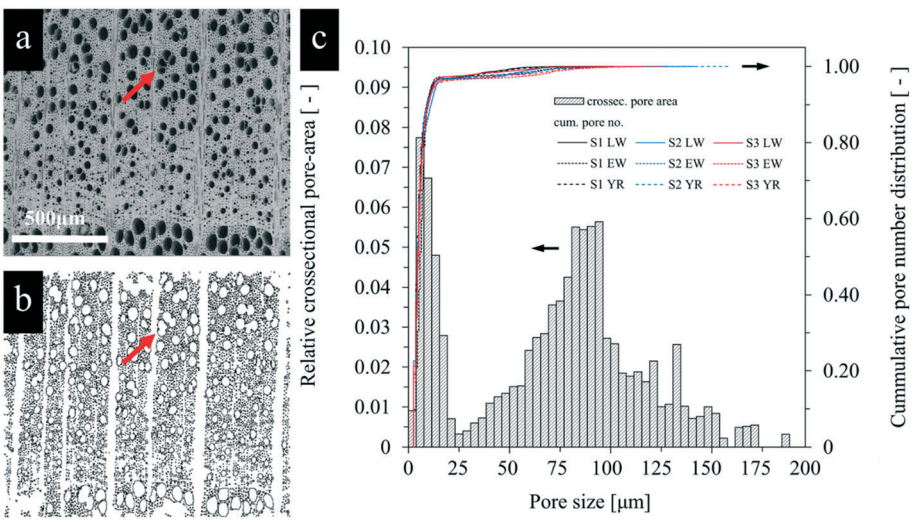

Fig. 3 (a) Typical SEM micrography, here the transition zone, used for the image analysis and (b) processed binary image. The red arrows indicate a vessel cluster. (c) Corresponding cross-sectional area distribution and cumulative percentage of pore number for all three samples over different regions labelled as earlywood (EW), latewood (LW), and a transition zone located on the year ring (YR).

of SiO_2, though, traces of aluminium, iron oxide, lime, magnesium, and sodium can also be present. Geological deposits of DE are obtained through mining, they are then crushed and milled to form a powder with the desired grain.[52]

To conduct image analysis of the wood cross-sections, a clean image of the surface, *i.e.* a clean wood cut, is required. This is usually obtained with microtome instruments or polishing. In reality, the wood cutting processes (such as circular saw cutting) are known to strongly affect the surface of the samples.[53] Cut wood surfaces are extremely rough. The high roughness is mainly caused by damaged cells or torn and collapsed cell wall fragments which can fill up or block the lumina of intact cells below the surface (see Fig. S6†). The characterisation of this porosity cannot be conducted with image analysis and would be extremely challenging with other techniques because it consists of a 30 μm layer with open porosity located on top of a porous bulk material. However, alternative measurements by intrusion porosimetry confirmed the results obtained from image analysis, while giving more information on smaller pores (<10 μm). As shown on Fig. S7,† a bimodal curve (centred around 20 μm and 100 μm) has been found through mercury porosimetry, the difference in relative volume coming from the ability of this technique to measure the porosity in the bulk in contrast to image analysis, which focuses on the surface.[54] According to these results, the porosity of the bulk is mostly described by pores of size 20 μm.

3.2. Performance parameters

3.2.1. Long-time behaviour and reutilisation. The pressure and flow behaviour of the wood scaffold has been investigated in a long-time experiment. The results presented on Fig. 4 show that no steady state has been reached on this time span. On a shorter time span, however, a monotone function can be observed. Hence, the filtration test will be conducted in this steady-state gap (30 min from start) in order to externalise this effect.

Swelling of the samples while testing is suspected to be the cause of the observed decrease in flux and simultaneous increase in pressure over the experimental runtime. Water molecules can interact with hydroxyl groups present on the wood cell wall through hydrogen bonding, making wood a hygroscopic material.[55] This causes the cell walls to swell, followed by an overall increase in the dimension of the sample. The wood discs mainly expand in the tangential direction, while the custom-made filter apparatus holding the wood disc constrains this swelling. The wood cell wall swelling and the restrained dimensional change likely lead to smaller lumen opening and potentially in some cases to a complete sealing of the smaller wood pores. This phenomenon can therefore affect the overall porosity of the filter.[43] The results shown in Fig. 4 attest the reversibility of this process. On the right hand side of the graphic, the filtration resumed after drying the samples in an oven at 65 °C during 24 h, allowing the removal of bound water from the cell

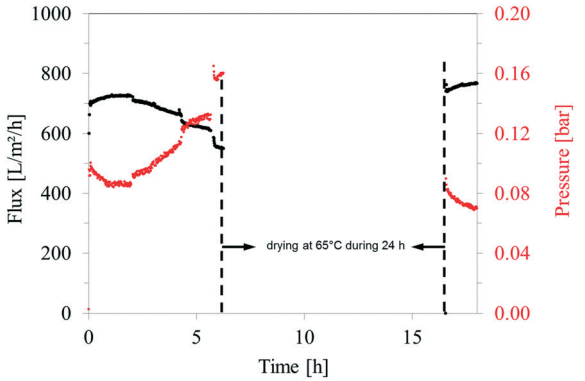

Fig. 4 Flux through the wood filter and corresponding pressure evolution during a long-time experiment, with a drying step in-between two filtration sequences.

wall.[56] Similar flux and pressure values have been observed after drying the sample, confirming the reversibility of the swelling.

3.2.2. Variability within the samples. The water conducting property of wood tissues can be investigated and quantified through the permeability k of the filter, defined as the transmittance of a media throughout the material. According to eqn (8), when the filtration area A is known, the permeability can be derived from the measured flux Q and pressure p measured during the experiment:

$$k = \frac{Q}{p} \Big/ A \tag{8}$$

The permeability has been determined for three samples and the results are plotted in Fig. 5. Although all samples have been cut from the same original material (*i.e.* same tree, and same region from the stem), natural wood variability induces some discrepancy in between samples. Due to the semi-ring porous nature of beech wood, the porosity, along with the size of the vessels, decreases over a year ring from earlywood to latewood.[49] With our sample sizes, we have an alternation between EW and LW regions, as shown in Fig. S8.† Hence, the proportion of earlywood with respect to latewood can influence the permeability.

In addition, the flow within the wood tissue might be hindered by various anatomical features. Pits between adjacent wood cells can split the flow in various channels. In the living tree, this behaviour is highly desired, as it ensures the water transport even following an injury obstructing a given area.[49] Due to the longitudinal length of our samples (1 mm) and knowing that the mean length of a single vessel element is about 560 μm, the filter is traversed by vessels assembled from two or more interconnected single elements.[27] The contacting interface at the extremity of single vessel elements can be a simple perforation (simple opening) or a more delicate lace-like structure (several smaller openings, see Fig. S9†).[34] These structures might be seen as obstacles to the circulation of fluids, since they offer a higher resistivity to the

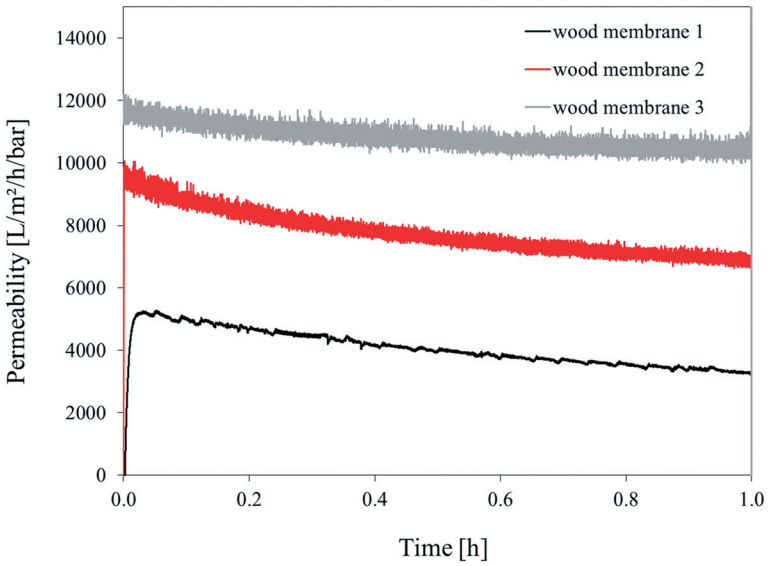

Fig. 5 Permeability changes during a short-term implementation (1 h) of three distinct wood filters.

flow.[57] As they are randomly distributed, their influence is difficult to quantify.

Regardless of the variability, the permeabilities of all wood filters were above 4000 L m^{-2} h^{-1} per bar. For comparison, synthetic ultrafiltration membranes are usually operated under 0.5–1.0 bar with ideal fluxes ranging from 50–100 L m^{-2} h^{-1}.[58,59] Commercially available microfiltration membranes typically work under a flux of 100 L m^{-2} h^{-1}.[60] The permeability of the wood filter exhibited at least 10 times the permeability expected from conventional polymeric or hybrid materials.

Through a slightly different approach, it is possible to link the permeability of the material with a specific media. The specific permeability of the material can be determined by applying Darcy's law. The validity of this approach has been investigated by Siau *et al.*,[23] who approximated a hardwood vessel to an open capillary running across the entire length of the wood samples. Furthermore, they assumed that due to their very small diameter when compared to the wood vessels, the flow through wood fibres and longitudinal parenchyma cells is insignificant. According to Kollmann *et al.*, the number of capillaries can be replaced by their area, which is proportional to the general size of the cross-section.[61] Thus, an expression generalising the implementation of Darcy's law to different wood types, without involving structural considerations can be developed (eqn (9)):

$$K = \frac{\eta \cdot Q}{A \cdot \Delta p} \tag{9}$$

where K = specific permeability, η = dynamic viscosity of the medium (here water, $\eta^{20°C} = 1.002 \times 10^{-6}$ Pa s), A = filtration area, Δp = pressure difference, and Q = flux. Moreover, specific permeability is the product of permeability and the dynamic viscosity of the fluid, thus its value relies only on the size and number of openings in the wood structure.[23]

The specific permeability has been calculated for the three samples, using the same dataset of flux and pressure, and has been found to be 37.57 ± 17.58 μm^3 μm^{-1}. The specific permeability of the wood filter is ten times higher when compared to common material used for sand filtration such as perlite (3.2 μm^3 μm^{-1}) or DE (3.6 μm^3 μm^{-1}), both being granular materials.[62] It can be compared to sintered metal fibre media, which have shown permeability up to 36 μm^3 μm^{-1}.[31]

3.3. Removal of silica particles

The predicted LRV of the wood filters are shown together with experimental results in Fig. 6. These predictions were calculated for the removal of particles with 5, 10, 15 and 20 μm diameters through physical sieving, using the pore sizes determined with our image analysis (see Fig. 3c).

For the smaller particle size, the experimental result is within the confidence interval of the prediction, indicating that the filtration proceeded *via* physical sieving. However, the values obtained for the 20 μm-sized particle rejection are about ten times higher than expected. Hence, at first glance, the filtration of bigger particles seems to involve other mechanisms, aside from physical sieving.

The integrity of the filter has been evaluated by a spiking test using the 20 μm particles. The variation of the fluorescence emissions from the feed and the permeate with time are shown in Fig. 7. For the initial feed concentration (5×10^5 particles per mL), the fluorescence emission measured was 38 514 ± 2667 AU. In the first 10 min, the filter was challenged with the matrix solution (no fluorescence). After switching to the matrix solution containing the particles, the emission of the feed increased rapidly and fluctuated for the next 10 min around 31 549 ± 1268 AU. Simultaneously, the

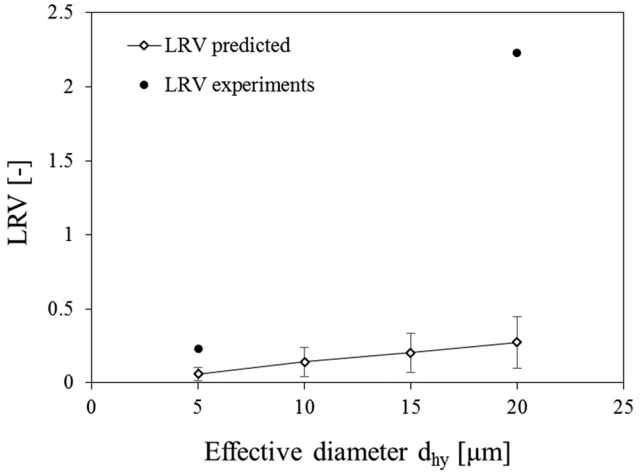

Fig. 6 Predicted log removal values (LRV) and LRV measured during the experiments with 5 μm and 20 μm sized microspheres, error bars represent 95% confidence interval.

emission of the permeate samples first displayed a value of 15 443 ± 7195 AU before rapidly decreasing. During this test, the flow quickly dropped and the pressure increased. After switching back to the matrix solution at a runtime of 20 min, the fluorescence emission measurements of the feed samples decreased slowly to an emission value of 1718 ± 312 AU and the flow and pressure stabilised.

According to the result of the spiking test, a steady-state in the removal efficiency was reached within 10 min of the filtration test. The same test has been performed with the 5 μm particles, shown in Fig. S10.† However, due to the poor rejection, the steady-state could not be clearly identified.

The rejection of 5 and 20 μm-sized particles has been investigated in short-term experiments as well. The variation in the fluorescence emission of the feed and the permeate are plotted alongside the log removal values over the duration of the experiment in Fig. 8. During the rejection experiment with the 5 μm-sized microspheres, the LRV stabilised around 0.2 after 30 min of runtime, reaching a maximum of 0.23. The final LRV correspond to the removal of 42% of the particles.

With the 20 μm particles, the stabilisation of the LRV at 2.2 was faster (1 min). No particle could be detected in the permeate at the end of the experiment, confirming the retention of 99% of the particles, as indicated by the LRV.

The decrease in flow and pressure occurring during these experiments can be related to the formation of a filter cake on top of the filter. Indeed, the particle of size 20 μm are bigger than the mean pore size found by image analysis. Consequently, the microspheres start accumulating onto the surface of the wood, forming bigger agglomerates that give rise to a filter cake. Within this layer, the particles are tightly packed, thus, forming a barrier to new particles coming from the feed stream. Although this effect was observed with both particle sizes, the filter cake made of 20 μm microspheres was more important, forming a thick film on top of the filter, indicating a high concentration of particles, as shown on Fig. S8.† The effect of a particle layer significantly increased the filtration efficiency, especially for 20 μm particles.

As shown in Fig. S6,† the morphology of a real wood surface (*i.e.* after circular saw cutting) is very different from a microtomed surface. While the surface still has pores, it is likely that smaller pores result from the arrangement of shredded and torn fibres, also leading to a more tortuous path for microparticles. We further tested this hypothesis

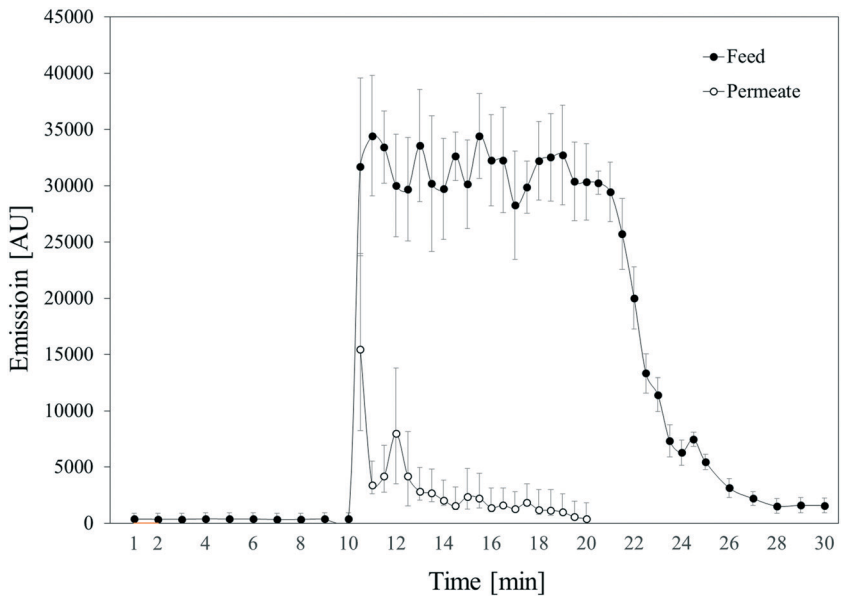

Fig. 7 Time-dependent spiking test conducted with microspheres of 20 μm size. The sampling has been performed at the inlet (feed) and outlet (permeate) of the filter, error bars represent 95% confidence interval.

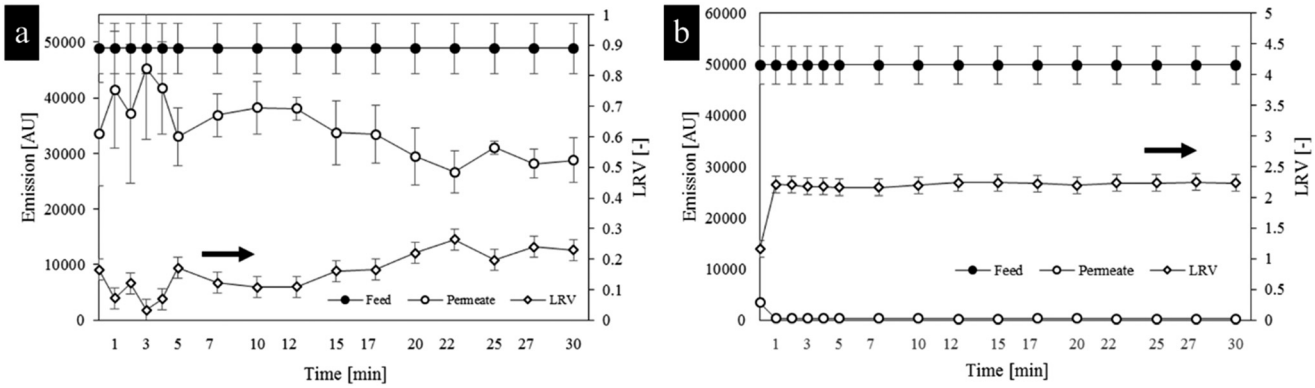

Fig. 8 Log removal values together with the fluorescent emission of the permeate and feed recorded during rejection experiments using (a) 5 μm and (b) 20 μm sized microspheres, error bars represent 95% confidence interval.

through a simple experiment. We polished (microtomed) the filter surface exposed to the feed, and filtrated 20 μm-sized particles. As shown in Fig. S11,† this did not lead to the retention of particles on the surface of the material, and prevented the formation of a filter cake. Hence, it is likely that the natural roughness gained through mechanical cutting helps trapping the particles on the surface.

The presence of pores bigger than 20 μm, and, hence, bigger than 5 μm, is attested in the distribution. These pores are susceptible to let the microsphere particles pass through during the filtration experiments, thus, decreasing the rejection capacity of the filter. While a fraction of the particles is retained at the filter surface, the microscopy investigation of the samples used for the filtration shown in Fig. 9 clearly shows that some particles are trapped within the material. Therefore, the particle retention seems to result from a surface effect and from another physical sieving inside the wood tissue.

As shown in Fig. 9, all particles penetrating inside the wood section have been immobilised into vessels. As stated before, the vessels traversing our 1 mm thick filters are constituted by at least two vessel elements. Consequently, each vessel contains at least one connection between these two individual vessel elements. In the case of a simple perforation, transport of liquids and small particles should be unhindered. However, when a scalariform perforation is encountered, the opening sizes are smaller, and small particles might be retained by these structures. This is another plausible explanation for the retention of 5 and 20 μm particles inside the wood filter.

As an alternative to hardwood, the capacity of a softwood (spruce) to uphold particles has also been investigated. We have observed that spruce wood was able to remove 20 μm-sized particles. Similarly to beech, a clean surface provided the access to the bulk of the material, whereas a rough surface, resulting from mechanical cutting, was able to retain

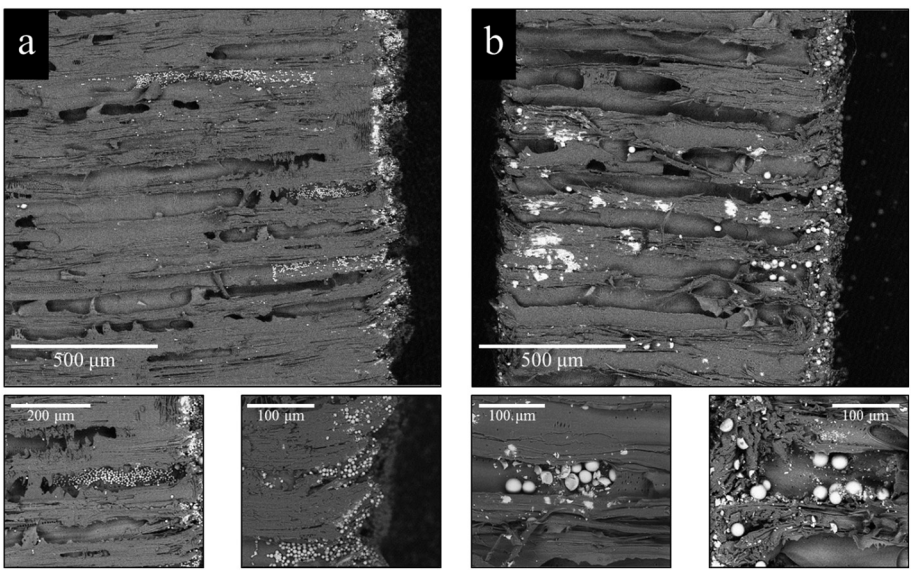

Fig. 9 Microscopy images of length-cut samples after filtration of (a) 5 μm particles and (b) 20 μm particles. Details give a zoom of the region where particles have accumulated.

particles on top of the surface (Fig. S12†). In terms of removal efficiency (see Fig. S13†), spruce filters (polished: 98%; rough: 96%) show similar results with beech (polished: 96%; rough: 98%).

Wood filters have shown an efficient removal of 20 μm-sized particles. For comparison, the removal of particles within this size range is performed through micro-filtration setups equipped with a membrane filtration unit or a fixed-bed packed with granular material.

As a practical example, the removal of *Cryptosporidium* oocysts, which are micron-sized protozoan cysts (4–15 μm) negatively charged in raw water, can be performed through microfiltration or the use of a packed bed of DE.[63,64] The LRV for the oocyst ranges between 4.2–4.9 when using microfiltration, and 1.7–2.2 with DE. However, it was shown that higher flowrate might increase the uptake of the oocyst to ~6 log values.[65] As the wood material exhibits a high permeability, increasing the operating pressure could be envisaged while aiming at enhancing the removal efficiency. When implemented in a pilot plant, the DE filters have shown LRV of about 3.8–3.9, which corresponds to 99.9–99.99% of removal.[50] Hence, the permeability is an important criteria and the wood filter has shown a higher permeability than DE. This would allow replacing a slow fixed-bed with a high flow filter unit, showing good mechanical integrity and facilitated implementation.

4. Conclusion and outlook

We investigated the potential of beech wood to filter micron-sized particles from water, based on physical sieving. The intrinsic porosity of this wood species is well suited for this application, without significant pressure loss over the filter. The ability of the filter to uphold particles has been assessed through filtration of particles with different sizes of 5 and 20 μm. Due to their size and surface charge, the silica particles could be considered as suitable surrogates to *Cryptosporidium* oocysts and *Giardia* cysts. The ζ-potential of the surrogates being close to the one of wood, electrostatic interactions could be excluded, meaning that only physical sieving is taking place. Due to the swelling, the permeability of the material changed over time. However, this phenomenon has been shown to be reversible upon drying the filter to remove free and bound water. The wood filter were characterised by image analysis to determine the pore size distribution, which exhibited a bimodal curve. These results have been used to calculate a theoretical rejection capacity, which could help understanding the rejection mechanisms.

The rough surface of the material has shown to be able to trap particles of both sizes, with formation of a filter cake. The deviation from the predicted rejection indicates a strong influence of the filter cake on the rejection of 20 μm-sized particles. Indeed, the impact of the filter cake was significant for this particle size, suggesting that the accumulation of the particles on top of the filter yielded a structure with smaller pore sizes than the wood.

The results gathered in this study support the implementation of beech wood as a filter. However, efficiency has been shown only for particles with a 20 μm diameter. Further studies have to be conducted for other particle sizes, mimicking other pollutants, in particular bacteria. The great variety of tree species allows investigating other materials with a wide range of pore sizes and pore distributions. In addition, the surface charges of wood can be tuned through chemical modification in order to increase the removal of smaller particles by electrostatic forces or chemical binding. It is also possible to protect the wood sample against pathogenic invasion from the raw water, and especially mould. However, wood being a cheap and readily available resource, we advise against extensive processing of the material and would rather suggest using the filter as a disposable one. Although the implementation in a dead-end flow was successful, the decrease in permeability over time is an issue that should be addressed in future studies as well.

Conflicts of interest

The authors declare no competing financial interest.

Acknowledgements

We acknowledge support from the Scientific Centre for Optical and Electron Microscopy (ScopeM, ETHZ). This research work was supported by the Swiss National Science Foundation (Grant No. 160041).

References

1 N. L. Le and S. P. Nunes, Materials and membrane technologies for water and energy sustainability, *Sustainable Mater. Technol.*, 2016, 7, 1–28.
2 D. M. Warsinger, S. Chakraborty, E. W. Tow, M. H. Plumlee, C. Bellona, S. Loutatidou, L. Karimi, A. M. Mikelonis, A. Achilli, A. Ghassemi, L. P. Padhye, S. A. Snyder, S. Curcio, C. D. Vecitis, H. A. Arafat and V. J. H. Lienhard, A review of polymeric membranes and processes for potable water reuse, *Prog. Polym. Sci.*, 2018, **81**, 209–237.
3 S. L. Loo, A. G. Fane, W. B. Krantz and T. T. Lim, Emergency water supply: A review of potential technologies and selection criteria, *Water Res.*, 2012, **46**(10), 3125–3151.
4 Z. Yang, X. H. Ma and C. Y. Y. Tang, Recent development of novel membranes for desalination, *Desalination*, 2018, **434**, 37–59.
5 R. Das, M. E. Ali, S. B. Abd Hamid, S. Ramakrishna and Z. Z. Chowdhury, Carbon nanotube membranes for water purification: A bright future in water desalination, *Desalination*, 2014, **336**, 97–109.
6 G. Szekely, M. F. Jimenez-Solomon, P. Marchetti, J. F. Kim and A. G. Livingston, Sustainability assessment of organic solvent nanofiltration: from fabrication to application, *Green Chem.*, 2014, **16**(10), 4440–4473.
7 T. B. Hofstetter, C. Capello and K. Hungerbuhler, Environmentally preferable treatment options for industrial

waste solvent management - A case study of a toluene containing waste solvent, *Process Saf. Environ. Prot.*, 2003, **81**(B3), 189–202.

8 J. D. Burgal, L. Peeva and A. Livingston, Towards improved membrane production: using low-toxicity solvents for the preparation of PEEK nanofiltration membranes, *Green Chem.*, 2016, **18**(8), 2374–2384.

9 Q. Fu, F. Ansari, Q. Zhou and L. A. Berglund, Wood Nanotechnology for Strong, Mesoporous, and Hydrophobic Biocomposites for Selective Separation of Oil/Water Mixtures, *ACS Nano*, 2018, **12**(3), 2222–2230.

10 S. Heydarifard, Y. Pan, H. M. Xiao, M. Nazhad and O. Shipin, Water-resistant cellulosic filter containing non-leaching antimicrobial starch for water purification and disinfection, *Carbohydr. Polym.*, 2017, **163**, 146–152.

11 H. Sehaqui, U. P. de Larraya, P. Liu, N. Pfenninger, A. P. Mathew, T. Zimmermann and P. Tingaut, Enhancing adsorption of heavy metal ions onto biobased nanofibers from waste pulp residues for application in wastewater treatment, *Cellulose*, 2014, **21**(4), 2831–2844.

12 Y. Li, H. Xiao, Y. Pan and L. Wang, Novel Composite Adsorbent Consisting of Dissolved Cellulose Fiber/Microfibrillated Cellulose for Dye Removal from Aqueous Solution, *ACS Sustainable Chem. Eng.*, 2018, **6**(5), 6994–7002.

13 F. Wang, Y. Pan, P. Cai, T. Guo and H. Xiao, Single and binary adsorption of heavy metal ions from aqueous solutions using sugarcane cellulose-based adsorbent, *Bioresour. Technol.*, 2017, **241**, 482–490.

14 A. Saeed, M. W. Akhter and M. Iqbal, Removal and recovery of heavy metals from aqueous solution using papaya wood as a new biosorbent, *Sep. Purif. Technol.*, 2005, **45**(1), 25–31.

15 L. Cutillas-Barreiro, R. Paradelo, A. Igrexas-Soto, A. Núñez-Delgado, M. J. Fernández-Sanjurjo, E. Álvarez-Rodriguez, G. Garrote, J. C. Nóvoa-Muñoz and M. Arias-Estévez, Valorization of biosorbent obtained from a forestry waste: Competitive adsorption, desorption and transport of Cd, Cu, Ni, Pb and Zn, *Ecotoxicol. Environ. Saf.*, 2016, **131**, 118–126.

16 K. Periasamy and C. Namasivayam, Removal of copper(II) by adsorption onto peanut hull carbon from water and copper plating industry wastewater, *Chemosphere*, 1996, **32**(4), 769–789.

17 L. Huang, Z. Ou, T. B. Boving, J. Tyson and B. Xing, Sorption of copper by chemically modified aspen wood fibers, *Chemosphere*, 2009, **76**(8), 1056–1061.

18 M. Argun, S. Dursun, C. Ozdemir and M. Karatas, Heavy Metal Adsorption by Modified Oak Sawdust: Thermodynamics and Kinetics, *J. Hazard. Mater.*, 2007, **141**(1), 77–85.

19 S. Vitas, T. Keplinger, N. Reichholf, R. Figi and E. Cabane, Functional lignocellulosic material for the remediation of copper(II) ions from water: Towards the design of a wood filter, *J. Hazard. Mater.*, 2018, **355**, 119–127.

20 F. Chen, A. S. Gong, M. Zhu, G. Chen, S. D. Lacey, F. Jiang, Y. Li, Y. Wang, J. Dai, Y. Yao, J. Song, B. Liu, K. Fu, S. Das and L. Hu, Mesoporous, Three-Dimensional Wood Membrane Decorated with Nanoparticles for Highly Efficient Water Treatment, *ACS Nano*, 2017, **11**(4), 4275–4282.

21 A. Auckenthaler, U. von Gunten, M. Sturzenegger, M. Boller, T. Egli, W. Pronk and P. Studer, *Procédés reconnus destinés au traitement de l'eau potable*, Office fédéral de la santé publique (OFSP), 2010.

22 B. Skibinski, P. Muller and W. Uhl, Rejection of submicron sized particles from swimming pool water by a monolithic SiC microfiltration membrane: Relevance of steric and electrostatic interactions, *J. Membr. Sci.*, 2016, **499**, 92–104.

23 J. F. Siau, *Flow in Wood*, Syracuse University Press, New York, 1971.

24 R. Shmulsky and P. D. Jones, *Forest products and wood science : an introduction*, Wiley-Blackwell, Chichester, West Sussex, U.K., Ames, Iowa, 6th edn, 2011, p xvii, p. 477.

25 D. Fengel and G. Wegener, *Wood: chemistry, ultrastructure, reactions*, De Gruyter, 2011.

26 T. T. Kozlowski and S. G. Pallardy, *Physiology of Woody Plants*, Elsevier Science, 1996.

27 H. Süss and W. R. Müller-Stoll, Längenänderungen einiger Holzelemente der Rotbuche (Fagus sylvatica L.) in Abhängigkeit von Stammhöhe und Himmelsrichtung, *Holz Roh- Werkst.*, 1984, **42**(11), 409.

28 K. S. Buchmüller, Jahrringcharakteristik und Gefässlängen in Fagus sylvatica L, *Vierteljahresschr. Naturforsch. Ges. Zürich*, 1986, **131**(3), 161–182.

29 M. S. H. Boutilier, J. Lee, V. Chambers, V. Venkatesh and R. Karnik, Water Filtration Using Plant Xylem, *PLoS One*, 2014, **9**(2), e89934.

30 M. L. Sens, M. L. Emmendoerfer and L. C. Muller, Water filtration through wood with helical cross-flow, *Desalin. Water Treat.*, 2015, **53**(1), 15–26.

31 E. S. Tarleton and R. J. Wakeman, 2 - Filter media, in *Solid/Liquid Separation*, ed. E. S. Tarleton and R. J. Wakeman, Butterworth-Heinemann, Oxford, 2007, pp. 78–125.

32 M. Plötze and P. Niemz, Porosity and pore size distribution of different wood types as determined by mercury intrusion porosimetry, *Eur. J. Wood Wood Prod.*, 2011, **69**(4), 649–657.

33 F. H. Schweingruber, *Mikroskopische Holzanatomie: Formenspektren mitteleuropäischer Stamm- und Zweighölzer zur Bestimmung von rezentem und subfossilem Material*, Eidgenössische Forschungsanstalt fur Wald, Schnee und Landschaft, 1990.

34 R. A. Parham and R. L. Gray, Formation and Structure of Wood, in *The Chemistry of Solid Wood*, ed. R. Rowell, American Chemical Society, 1984, vol. 207, pp. 3–56.

35 B. Davies, Edme Mariotte 1620-1684, *Phys. Educ.*, 1974, **9**(4), 275.

36 M. Kireš, Mariotte Bottle with Side Openings, *Phys. Teach.*, 2006, **44**(6), 388–389.

37 S. C. J. M. Van Hoof, L. Broens, A. Nahrstedt, S. Panglisch and R. Gimbel in *Development of a new integrity testing system 5th Membranes in Drinking and Industrial Water Production*, Mulheim an der Ruhr, 2002, pp. 22–26.

38 H. Guo, Y. Wyart, J. Perot, F. Nauleau and P. Moulin, Low-pressure membrane integrity tests for drinking water treatment: A review, *Water Res.*, 2010, **44**(1), 41–57.

39 C. A. Schneider, W. S. Rasband and K. W. Eliceiri, NIH Image to ImageJ: 25 years of image analysis, *Nat. Methods*, 2012, **9**, 671–675.
40 I. Masselin, L. Durand-Bourlier, J.-M. Laine, P.-Y. Sizaret, X. Chasseray and D. Lemordant, Membrane characterization using microscopic image analysis, *J. Membr. Sci.*, 2001, **186**(1), 85–96.
41 Y. Wyart, G. Georges, C. Deumié, C. Amra and P. Moulin, Membrane characterization by microscopic methods: Multiscale structure, *J. Membr. Sci.*, 2008, **315**(1), 82–92.
42 V. Singh, M. K. Purkait, V. K. Chandaliya, P. P. Biswas, P. K. Banerjee and C. Das, Development of membrane based technology for the separation of coal from organic solvent, *Desalination*, 2012, **299**, 123–128.
43 M. Zauer, S. Hempel, A. Pfriem, V. Mechtcherine and A. Wagenführ, Investigations of the pore-size distribution of wood in the dry and wet state by means of mercury intrusion porosimetry, *Wood Sci. Technol.*, 2014, **48**, 1229–1240.
44 L. F. Muff, T. Luxbacher, I. Burgert and B. Michen, Investigating the time-dependent zeta potential of wood surfaces, *J. Colloid Interface Sci.*, 2018, **518**, 165–173.
45 A. V. Delgado, F. González-Caballero, R. J. Hunter, L. K. Koopal and J. Lyklema, Measurement and Interpretation of Electrokinetic Phenomena (IUPAC Technical Report), in *Pure and Applied Chemistry*, 2005, vol. 77, p. 1753.
46 Chemical analysis-Decision limit, detection limit and determination limit under repeatability conditions - Terms, methods, evaluation (in German), in *DIN-32645*, ed. D. D. I. F. Normung, Beuth Verlag, Berlin, 2008.
47 L. Zeman and M. Wales, Polymer Solute Rejection by Ultrafiltration Membranes, In *Synthetic Membranes: Volume II*, American Chemical Society, 1981, vol. 154, pp. 411–434.
48 R. Wagenführ, *Anatomie des Holzes*, VEB Fachbuchverlag, Leipzig, 1980.
49 P. Hass, F. Wittel, S. A. McDonald, F. Marone, M. Stampanoni, H. J. Herrmann and P. Niemz, Pore space analysis of beech wood: The vessel network, *Holzforschung*, 2010, **64**(5), 639–644.
50 J. E. Ongerth and P. E. Hutton, DE filtration to remove Cryptosporidium, *J. - Am. Water Works Assoc.*, 1997, **89**(12), 39–46.
51 P. G. Fields, In *Diatomaceous earth: Advantages and limitations*, Proceedings of the Seventh International Working Conference on Stored-Product Protection, 1998, vol. 1998, pp. 781–784.
52 R. Calvert, Diatomaceous earth, *J. Chem. Educ.*, 1930, **7**(12), 2829.
53 E. Magoss, General Regularities of Wood Surface Roughness, *Acta Silv. Lign. Hung.*, 2008, **4**, 81–93.
54 G. Herbert, Mercury Porosimetry: A General (Practical) Overview, *Part. Part. Syst. Charact.*, 2006, **23**(1), 9–19.
55 C. Skaar, Wood-Water Relationships, in *The Chemistry of Solid Wood*, American Chemical Society, 1984, vol. 207, pp. 127–172.
56 A. Wagenführer and F. Scholz, *Taschenbuch der Holztechnik*, Carl Hanser Verlag, München, 2008.
57 M. A. Christman and J. S. Sperry, Single-vessel flow measurements indicate scalariform perforation plates confer higher flow resistance than previously estimated, *Plant, Cell Environ.*, 2010, **33**(3), 431–443.
58 M. Peter-Varbanets, J. Margot, J. Traber and W. Pronk, Mechanisms of membrane fouling during ultra-low pressure ultrafiltration, *J. Membr. Sci.*, 2011, **377**(1), 42–53.
59 Q. Gao, C.-Z. Wang, S. Liu, D. Hanigan, S.-T. Liu and H.-Z. Zhao, Ultrafiltration membrane microreactor (MMR) for simultaneous removal of nitrate and phosphate from water, *Chem. Eng. J.*, 2019, **355**, 238–246.
60 K. J. Howe and M. M. Clark, Fouling of Microfiltration and Ultrafiltration Membranes by Natural Waters, *Environ. Sci. Technol.*, 2002, **36**(16), 3571–3576.
61 F. Kollmann, Pores and pore content in wood, *Holz Roh-Werkst.*, 1987, 1–9.
62 P. Lu, J. E. Amburgey, V. R. Hill, J. L. Murphy, C. L. Schneeberger, M. J. Arrowood and T. Yuan, Removals of cryptosporidium parvum oocysts and cryptosporidium-sized polystyrene microspheres from swimming pool water by diatomaceous earth filtration and perlite-sand filtration, *J. Water Health*, 2017, **15**(3), 374–384.
63 K. Shaw, S. Walker and B. Koopman, Improving Filtration of Cryptosporidium, *J. - Am. Water Works Assoc.*, 2000, **92**(11), 103–111.
64 W. Q. Betancourt and J. B. Rose, Drinking water treatment processes for removal of Cryptosporidium and Giardia, *Vet. Parasitol.*, 2004, **126**(1), 219–234.
65 J. E. Ongerth and P. E. Hutton, Testing of Diatomaceous Earth Filtration for Removal of Cryptosporidium Oocysts, *J. - Am. Water Works Assoc.*, 2001, **93**(12), 54–63.